Angewandte
Eine Zeitschrift der Gesellschaft Deutscher Chemiker
Chemie

Supporting Information

Kinetics of the Antibody Recognition Site in the Third IgG-Binding Domain of Protein G

Supriya Pratihar[+], T. Michael Sabo[+], David Ban, R. Bryn Fenwick, Stefan Becker, Xavier Salvatella, Christian Griesinger, and Donghan Lee**

anie_201603501_sm_miscellaneous_information.pdf

Supporting Information

Supplementary Methods

Sample Preparation

Perdeuterated ^{15}N-labeled GB3 was expressed in *E. coli* adapted to 100% D_2O minimal medium supplemented with D_7-glucose as the carbon source and ^{15}N-NH_4Cl as the nitrogen source. Recombinant GB3 was purified as described before.[1] NMR experiments were performed on a 3 mM GB3 sample in 50 mM sodium phosphate buffer at pH 6.5, containing 100 mM NaCl and 0.05% sodium azide. RD experiments at temperatures ranging from 262 K to 275 K were carried out in capillary tubes to produce super-cooled conditions below the freezing point of water. Each glass capillary of 1 mm outer diameter (Wilmad, Buena, New Jersey) contained 25µl of the GB3 sample and 12 such capillaries were placed inside a 5 mm NMR sample tube.

NMR Spectroscopy

All the NMR measurements were recorded on a Bruker Avance III spectrometer, operating at a ^{1}H frequency of 600 MHz. Each spectrum for the RD measurements were recorded with 512 ($t_{2,max}$ = 65.5 ms) and 64 ($t_{1,max}$ = 31 ms) complex points in the direct (t_2) and indirect (t_1) dimension with four scans per t_1 increment. A recycle delay of 3 s was necessary for the high power $R_{1\rho}$ measurement. Backbone ^{15}N RD measurements were done following a two-point sampling scheme at relaxation delays of 2 ms and 125 ms, where the spin-lock RF field was varied from 1 kHz to 6 kHz. For backbone $^1H^N$ $R_{1\rho}$ RD measurements, the spin-lock RF field was varied from 1 kHz to 25 kHz. At every power level, the ^{1}H RF power was calibrated by measuring the 90^o pulse length of the water resonance. To minimize the pseudo-dispersion effect caused by NOE and ROE transfer effects, the tilt-angle (θ) was kept at 35.3^o ($\tan^{-1}[1/\sqrt{2}]$) for all the measurements by choosing the appropriate spin-lock offset relative to the center of the amide proton region (8 ppm).[2] This approach allows us to reach an effective RF field strength of

272,000 rad/s, which enabled us to detect single digit microsecond motion (3.4 μs). Before the spin-lock interval, all the spins under investigation were aligned with the off-resonance spin-lock field by applying a phase and amplitude modulated adiabatic RF pulse of 4 ms with a 100 kHz sweep width.[3] Rates were measured with a four point sampling scheme per RF amplitude, where the spin-lock delays were kept as 2, 45, 90 and 125 ms. The entire experiment was carried out in an interleaved fashion, where the spin-lock delay and RF amplitudes were varied randomly to have minimum heating effect (less than 1 K)

Data Processing and Analysis

The interleaved spectra were separated and co-added using a PERL script (in house) and were processed with NMRPipe.[4] Peak intensities for each spectrum were obtained using the model based batch-integration method implemented in the Computer Aided Resonance Assignment (CARA) program.[5] $R_{1\rho}$ values at each spin-lock frequency were determined by fitting the intensities at different spin-lock delays to a single exponential equation $\left(I_t = I_0 * \exp[R_{1\rho} * t]\right)$ and the corresponding errors were obtained from the residual of the four point fits. The effective spin-lock field (ω_{eff}) and the average $R_{1\rho}$ values were calculated following the previously described method.[2] Residues that showed a difference in $R_{1\rho}$ between the maximum and minimum spin-lock frequency of more than 2 s^{-1} were considered to exhibit significant chemical exchange and fitted to the equation,

$$\frac{R_{1\rho}}{\sin^2\theta} = R_2 + \frac{\Phi_{ex} * \tau_{ex}}{\left(1 + \tau_{ex}^2 * \omega_{eff}^2\right)} \quad (1)$$

in order to extract the intrinsic transverse relaxation rate (R_2), the chemical shift variance (φ_{ex}) and the exchange lifetime (τ_{ex}). Errors for the fitted parameters were calculated by a Monte Carlo simulation with 500 runs. $R_{1\rho}$ RD data from each temperature was fitted with equation 1 following a Akaike Information Criterion (AIC_C) based clustering approach (in house) and the

minimum AIC_C value was achieved when all the RD curves were fitted to single global timescale. R_2 and ϕ_{ex} were considered as individual parameters for each residue during the fitting process and they are listed in Supplementary Table S1. Results, obtained from individual fitting of τ_{ex} are listed in Supplementary Table S2. The global τ_{ex} obtained at various temperatures was then fitted with the Arrhenius equation to estimate the activation energy for the global exchange process,

$$\ln(\tau_{ex}) = \left(\frac{E_a}{RT}\right) - \ln(A) \quad (2)$$

where E_a and A are the activation energy and the attempt frequency, respectively.

The Eyring equation can also be used to determine the free energy and exchange rate (see Figure S1 for a plot of $\frac{k_{ex}}{T}$ vs $\frac{1}{T}$):

$$\ln\left(\frac{k_{ex}}{T}\right) = -\left(\frac{\Delta G}{RT}\right) + \ln(\frac{k_B}{\hbar}) \quad (3)$$

where k_B is Boltzmann's constant, $\hbar$ is Planck's constant, and ΔG is the Gibb's free energy. Based on a linear fit of data in figure S1, the Gibb's free energy was calculated as 60.9 ± 5.0 kJ/mol and τ_{ex} at physiological temperature (310 K) was extrapolated to be 409 ± 126 ns.

ERMD Generation

The RDC restrained ensemble was generated using ensemble restrained molecular dynamics for GB3 using six sets of previously published NH and CαHα RDCs,[6] with errors of 0.1 and 0.2 Hz respectively. Calculations were performed using the ERNST method[7] to produced twenty 64 member ensembles, which were combined to obtain a final ensemble of 640 members.

Table S1: Global fits for the exchange lifetime (τ_{ex}), conformational amplitude of motion ($\mathbf{\Phi}_{ex}$) and intrinsic transverse relaxation rate (R_2^0) obtained from the high power amide proton $R_{1\rho}$ RD experiment on GB3. To derive the parameters, the experimental $R_{1\rho}$ values were fitted to equation 1 following an Akaike Information Criterion (AIC_C) based clustering approach.

residue		G9	K10	T11	L12	K13
262 K	τ_{ex} (µs)	35.9 ± 1.3				
	φ_{ex} (10^3 rad^2.s^{-2})	735 ±18	603 ± 17	472 ± 23	1706 ± 63	309 ± 12
	R_2^0 (s^{-1})	22.7 ± 0.2	31.9 ± 0.2	59.6 ± 0.2	42.3 ± 0.5	20.6 ± 0.1
265 K	τ_{ex} (µs)	28.5 ± 1.1				
	φ_{ex} (10^3 rad^2.s^{-2})	605 ± 17	670 ± 24	287 ± 22	1770 ± 49	310 ± 12
	R_2^0 (s^{-1})	20.9 ± 0.1	28.0 ± 0.2	53.5 ± 0.2	40.3 ± 0.3	18.8 ± 0.1
269 K	τ_{ex} (µs)	15.6 ± 0.8				
	φ_{ex} (10^3 rad^2.s^{-2})	488 ± 28	542 ± 29	258 ± 23	1238 ± 64	209 ± 16
	R_2^0 (s^{-1})	18.1 ± 0.2	24.6 ± 0.2	44.1 ± 0.2	34.1 ± 0.4	16.5 ± 0.2
275 K	τ_{ex} (µs)	9.1 ± 0.4				
	φ_{ex} (10^3 rad^2.s^{-2})	357 ± 45	625 ± 52	139 ± 55	1342 ± 97	255 ± 32
	R_2^0 (s^{-1})	15.4 ± 0.3	19.9 ± 0.2	33.7 ± 0.4	26.9 ± 0.4	13.6 ± 0.2

Table S2: Individual fits for the exchange lifetime (τ_{ex}), conformational amplitude of motion ($\mathbf{\Phi}_{ex}$) and intrinsic transverse relaxation rate (R_2^0) obtained from the high power amide proton $R_{1\rho}$ RD experiment on GB3.

residue		G9	K10	T11	L12	K13
262 K	τ_{ex} (µs)	34.3 ± 1.2	48.9 ± 3.5	31.2 ± 3.1	35.4 ± 1.6	36.4 ± 2.3
	φ_{ex} (10^3 rad^2.s^{-2})	756 ± 15	521 ± 15	517 ± 43	1720 ± 66	307 ± 14
	R_2^0 (s^{-1})	22.6 ± 0.1	32.6 ± 0.2	59.3 ± 0.3	45.2 ± 0.5	20.6 ± 0.1
265 K	τ_{ex} (µs)	27.8 ± 0.7	33.9 ± 2.1	16.9 ± 3.1	28.3 ± 1.3	27.7 ± 1.7
	φ_{ex} (10^3 rad^2.s^{-2})	616 ± 14	598 ± 26	460 ± 92	1780 ± 54	317 ± 14
	R_2^0 (s^{-1})	20.8 ± 0.1	28.5 ± 0.2	52.6 ± 0.5	40.2 ± 0.4	18.7 ± 0.1
269 K	τ_{ex} (µs)	15.7 ± 1.2	21.4 ± 2.1	6.8 ± 1.6	15.3 ± 1.0	14.1 ± 1.8
	φ_{ex} (10^3 rad^2.s^{-2})	484 ± 39	405 ± 35	784 ± 224	1263 ± 89	233 ± 35
	R_2^0 (s^{-1})	18.2 ± 0.2	25.3 ± 0.2	42.2 ± 0.7	34.0 ± 0.4	16.4 ± 0.2
275 K	τ_{ex} (µs)	7.6 ± 2.1	12.5 ± 1.9	5.3 ± 10.6	8.7 ± 0.4	7.5 ± 1.8
	φ_{ex} (10^3 rad^2.s^{-2})	451 ± 152	422 ± 72	328 ± 166	1404 ± 107	327 ± 112
	R_2^0 (s^{-1})	15.1 ± 0.6	20.7 ± 0.3	33.1 ± 0.7	26.7 ± 0.4	13.4 ± 0.4

Table S3. Trans-hydrogen bond scalar couplings ($^{3h}J_{NC'}$) for GB3.

N	C'	$^{3h}J_{NC'}$(Hz)
3	18	0.72
4	50	0.42
5	16	0.75
7	14	0.65
8	54	0.77
9	12	0.40
16	5	0.43
18	3	0.43
20	1	0.51
28	24	0.18
29	25	0.22
31	27	0.73
32	28	0.19
33	29	0.20
34	30	0.58
36	32	0.59
37	33	0.19
39	34	0.31
44	53	0.59
46	51	0.50
51	46	0.23
52	4	0.80
53	44	0.55

$^{3h}J_{NC'}$ measurements were carried out on a sample of 5 mM ^{15}N,^{13}C-labeled GB3, in 50 mM phosphate buffer, pH 5.5. We utilized the previously reported 2D long-range TROSY-HNCO experiment to measure $^{3h}J_{NC'}$.[8] All the NMR measurements were recorded on a Bruker Avance III spectrometer, operating at a ^{1}H frequency of 700 MHz. Each spectrum was recorded with 1024 ($t_{2,max}$ = 105 ms) and 50 ($t_{1,max}$ = 23.7 ms) complex points in the direct (t_2) and indirect (t_1) dimension with 128 and 512 scans per t_1 increment, for the reference and cross measurements, respectively. The spectra were processed with NMRPipe[4] and the peak intensities were obtained using the Computer Aided Resonance Assignment (CARA) program.[5] $^{3h}J_{NC'}$ was calculated as previously described.[8]

Table S4. Validation of Static and Ensemble Representations of GB3 Assessed by the Level of Agreement with NMR Experimental Data[a]

Scalar Couplings[b]

	Static				Ensemble				
	1IGD[c]	2OED[d]	New[e]		ERMD[f]	2LUM[g]	B/*D*/S^2_{LS} [h]	EM8[i]	ORIUM[j]
$^{3h}J_{NC'}$[k]	0.38	0.30	0.32		**0.22**	0.62	0.52	0.43	n.a.
$^{3}J_{H^N H^\alpha}$[l]	0.12	0.09	0.09		0.06	**0.05**[l]	0.06	0.07	0.11[m]
$^{3}J_{H^N C'}$[l]	0.39	0.27	0.26		0.25	**0.22**[l]	0.23	0.31	n.a.
$^{3}J_{H^N C^\beta}$[l]	0.19	0.15	0.14		**0.10**	0.16[l]	0.12	0.15	n.a.
$^{3}J_{C'C'}$[n]	0.22	0.16	0.12		0.15	0.21	**0.08**	0.19	n.a.

Cross-Correlated Relaxation Rates[o]

	Static				Ensemble				
	1IGD	2OED	New		ERMD	2LUM	B/*D*/S^2_{LS}	EM8	ORIUM
$\Gamma_{NH^N(i)/NH^N(i+1)}$[p]	0.19	0.19	0.15		**0.13**	0.21	**0.13**	0.15	0.14
$\Gamma_{NH^N(i)/C^\alpha H^\alpha(i)}$[p]	0.19	0.13	0.12		**0.09**	0.14	0.11	0.17	0.13
$\Gamma_{C^\alpha H^\alpha(i-1)/NH^N(i)}$[p]	0.19	**0.12**	0.14		0.14	0.25	**0.12**	**0.12**	0.14
$\Gamma_{C^\alpha H^\alpha(i-1)/C^\alpha H^\alpha(i)}$[p]	**0.19**	**0.19**	0.21		**0.19**	0.26	0.20	0.21	0.21

Residual Dipolar Couplings[q]

	Static				Ensemble				
	1IGD	2OED	New		ERMD	2LUM	B/*D*/S^2_{LS}	EM8	ORIUM
$D_{NH^N}/D_{C^\alpha H^\alpha}$[r]	0.16	0.09	0.06[r]		0.03[r]	0.22	0.10	0.12[p]	**0.01**[r]
$D_{NH^N}/D_{C^\alpha H^\alpha}$[s]	0.18	0.15	**0.11**[s]		0.12	0.25	**0.11**	0.15	**0.11**
$D_{NH^N}/D_{C^\alpha H^\alpha}$[t]	0.15	0.07[t]	0.05[t]		0.06	0.18	**0.03**[t]	0.10	0.21
$D_{C^\alpha C'}$[t]	0.17	0.13[t]	0.09[t]		0.13	0.23	**0.07**[t]	0.15	n.a.
$D_{C'N}$[t]	0.33	0.25[t]	**0.20**[t]		**0.20**	0.28	**0.20**[t]	0.32	n.a.
D_{NH^N}[u]	0.16	0.11	**0.06**		0.08	0.22	0.10	0.10	0.33
$D_{C^\alpha C'}$[u]	0.18	0.12	**0.10**		0.13	0.26	**0.10**	0.17	n.a.
$D_{C'H^N}$[u]	0.28	0.25	0.22		**0.19**	0.28	0.24	0.25	n.a.
D_{NH^N}[v]	0.16	0.11	**0.06**[v]		0.09	0.22	0.11	0.10[v]	0.38
$D_{C^\alpha C'}$[v]	0.19	0.14	**0.10**[v]		0.13	0.26	0.11	0.18	n.a.

[a]The level of agreement between the NMR observables and the GB3 structural data is represented by a quality factor (Q) as calculated by the following equation[9]: $Q = \sqrt{\frac{\sum_i (X_i^{observable} - X_i^{structural})^2}{\sum_i (X_i^{observable})^2}}$. For each NMR observable, the structure(s) that produces the best agreement is shown in bold.

[b]The Karplus equation,[10] $A\cos^2\phi + B\cos\phi + C$, was used to back-calculate $^{3}J_{H^N H^\alpha}$, $^{3}J_{H^N C'}$, $^{3}J_{H^N C^\beta}$, and $^{3}J_{C'C'}$, where ϕ is the intervening torsion angle between the two nuclei and A, B, and C are the Karplus parameters taken from Ref. [11] for $^{3}J_{H^N C'}$ and $^{3}J_{H^N C^\beta}$ and from Ref. [12] for $^{3}J_{H^N H^\alpha}$ and $^{3}J_{C'C'}$. For the ensembles, an ensemble average was determined: $\langle A\cos^2\phi + B\cos\phi + C\rangle$. Hydrogen bond scalar couplings, $^{3h}J_{NC'}$, were back-calculated according to equation 4 from Ref. [13].

[c]X-ray structure[14]

[d]NMR structure[15]

[e]Newly refined NMR structure[16]

[f]Ensemble Restrained Molecular Dynamics (ERMD) 640 member ensemble calculated as described in this publication.

[g]Exact nuclear Overhauser effect (eNOE) 60 member ensemble[17]

[h]B-factor/RDC/S^2_{LS} 160 member ensemble[18]

[i]Expectation Maximization 500 member ensemble[19]

[j]ORIUM dynamically averaged structural data[20]

[k]Hydrogen bond scalar coupling data presented in Table S3.

[l]Scalar couplings from Ref. [11]. These three sets of scalar couplings were used in the refinement of 2LUM.

[m]Back-calculated using the relationship $\cos(\theta) = -0.163 + 0.819\cos(\phi - 60°)$, where θ is the angle between the NH^N and $C^\alpha H^\alpha$ vectors and ϕ is the backbone dihedral angle.[21]

[n]Scalar couplings from Ref. [16].

[o]Cross-correlated relaxation (CCR) rates were back calculated using the following equation,[22]

$\Gamma_{YH/ZH} = \left(\frac{\mu_0\hbar}{4\pi}\right)^2 \left(\frac{\gamma_Y\gamma_H}{r_{YH}}\right)\left(\frac{\gamma_Z\gamma_H}{r_{ZH}}\right)(3\cos^2\theta - 1)\frac{\tau_c}{5}$, where μ_0 is the magnetic susceptibility of vacuum, $\hbar$ is Planck's constant, γ_i is the gyromagnetic ratio of nucleus i, r_{iH} the distance between nucleus i and H, τ_c the correlation time of GB3 and θ the angle between bond vectors YH and ZH. For the ensembles, an ensemble average was determined, $\langle 3\cos^2\theta - 1\rangle$. When calculating

the Q-factors for the CCR rates, τ_c was optimized to maximize agreement with the experimental data and, thus, absorbs any dynamics associated with the individual vectors independent of each other, i.e. fast librational motions [23]. Table S5 reports the calculated τ_c for each structure and ensemble.

[p]CCR rates from Ref. [19].

[q]Residual Dipolar Couplings (RDCs) were back calculated using a single alignment tensor with ORIUM[20] and taking the ensemble averaged structural coordinates for the ensembles.

[r]RDCs from Ref. [6]. RDCs used in the refinement of New, ERMD, EM8 (only a subset) and ORIUM.

[s]RDCs from Ref. [16]. RDCs used in the refinement of New.

[t]RDCs from Ref. [15]. Alignment tensors for each condition were calculated from both D_{NH}^{N} and $D_{C^{\alpha}H^{\alpha}}$ simultaneously and used to back-calculate $D_{C^{\alpha}C'}$ and $D_{C'N}$. RDCs used in the refinement of 2OED, New and the B-factor/RDC/S^2_{LS} ensemble.

[u]RDCs from Ref. [24]. Alignment tensors for each condition were calculated from D_{NH}^{N} and used to back-calculate $D_{C^{\alpha}C'}$ and $D_{C'H}^{N}$.

[v]RDCs from Ref. [24]. Alignment tensors for each condition were calculated from D_{NH}^{N} and used to back-calculate $D_{C^{\alpha}C'}$. RDCs used in the refinement of New and EM8 (only a subset).

Table S5: Rotational correlation times (τ_c) in nanoseconds from fitting cross-correlated relaxation (CCR) rates to the indicated structure or ensemble.[a]

	Static[b]				Ensemble[c]				
	1IGD	2OED	New		ERMD	2LUM	B/D/S^2_{LS}	EM8	ORIUM
$\tau_{c(NH^N(i)/NH^N(i+1))}$[d]	2.37	2.41	2.38		2.69	2.81	2.55	2.57	2.49
$\tau_{c(NH^N(i)/C^\alpha H^\alpha(i))}$	2.87	2.93	2.92		3.17	3.18	3.04	3.19	3.10
$\tau_{c(C^\alpha H^\alpha(i-1)/NH^N(i))}$	2.99	2.91	2.88		3.13	3.15	2.98	3.08	3.05
$\tau_{c(C^\alpha H^\alpha(i-1)/C^\alpha H^\alpha(i))}$	2.92	2.95	2.92		3.11	2.97	2.96	3.10	3.12

[a]To estimate the rotational correlation (τ_c) time for protonated GB3, we utilized the TRACT measurement[25] at 298K, which yielded a value of 3.6 nsec. References for the static structures and the ensembles of GB3 are given in Table S4.

[b]The lower τ_c values for the static structures reflect the absorption of both fast and slow vector motions by τ_c during fitting.

[c]Assuming a uniform amount of fast librational motion (S_{libr}) for all bonds (defined as *A* or *B*) in GB3 ($S_{libr} = 0.95$)[23], the fitted τ_c values determined from the ensemble representations of GB3 can be scaled ($\tau_c / (S^A_{libr} S^B_{libr})$) in order to compare to the experimentally determined value for GB3. Based on the fitted τ_c values presented in this table for the CCR rates presumably measured with the same protonated GB3 sample (NH^N(i)/CαHα(i), CαHα(i-1)/NH^N(i), and CαHα(i-1)/CαHα(i)), we can report a range of 3.28 to 3.53 nsec, close to the value of 3.6 nsec measured in house on a different sample of GB3.

[d]Reference [19] indicates that both protonated and perdeuterated GB3 were used for the CCR measurements, though it does not mention which measurement utilized which form of GB3. Given that the only CCR rate a perdeuterated protein could provide information on is the NH^N(i)/NH^N(i+1) CCR rate, it stands to reason that different sample conditions, in addition to the perdeuteration, may explain the lower τ_c values for the NH^N(i)/NH^N(i+1) CCR rates when compared to the other 3 CCR rates which could have been measured on the same protonated GB3 samples.

Supplementary Figures

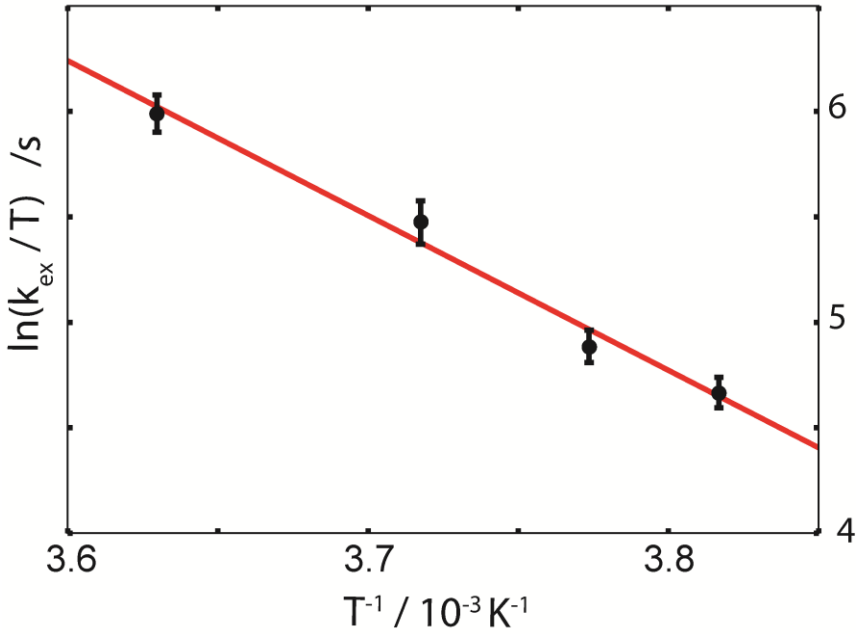

Figure S1. **Conformational exchange rates ($k_{ex} = 1/\tau_{ex}$), obtained from the global fitting of RD data, are plotted against temperature.** Solid red line indicates fits of the experimental data where the Gibbs free energy was calculated from the slope of the line as 60.9 ± 5.0 kJ/mol and the lifetime of conformational exchange at physiological temperature (310 K) was extrapolated to be 409 ± 126 ns.

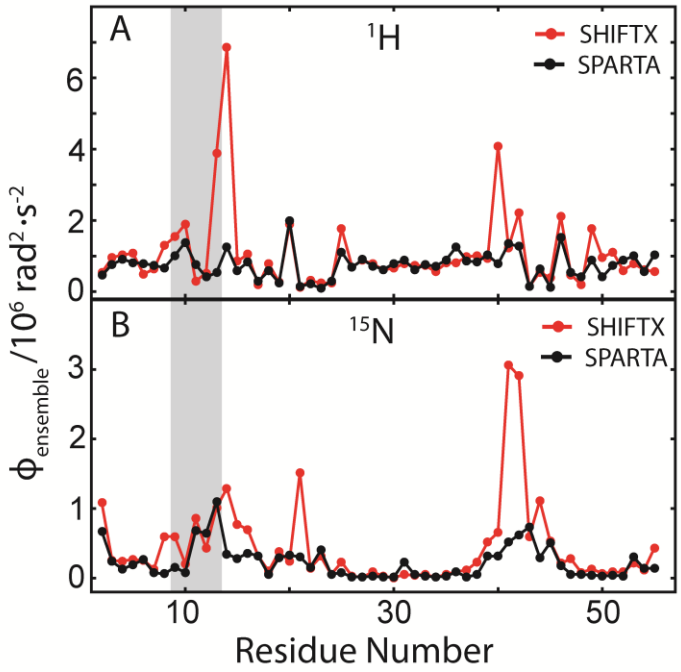

Figure S2. **Chemical shift variance prediction ($\varphi_{ensemble}$) from RDC derived structural ensemble of GB3.** ^{1}H (A) and ^{15}N (B) chemical shifts were extracted from the 640 member ERMD ensemble, using two different chemical shift predictors; SHIFTX[26] (red) and SPARTA[27] (black). The N-site jump model[28] was assumed for the calculation of $\varphi_{ensemble}$. The shaded region indicates the stretch of residues that display RD.

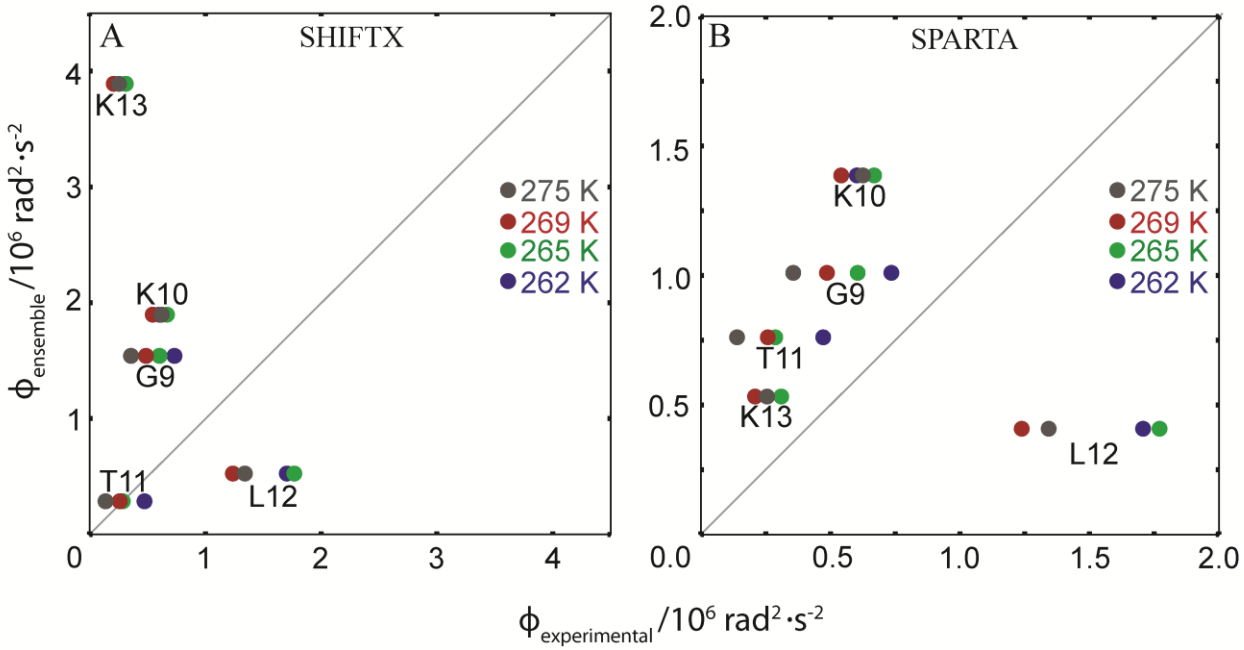

Figure S3. **Correlation plots of predicted versus experimental chemical shift variances.** The plots indicate that SHIFTX[26] (A) calculated CSV from the ERMD ensemble does not correlate with the experimental data with or without including L12 in the calculation. In the case of the SPARTA[27] (B) calculated CSV, removing L12 from the Pearson correlation calculation yields correlation coefficients of 0.74 at 262 K, 0.91 at 265 K, 0.94 at 269 K, and 0.88 at 275 K.

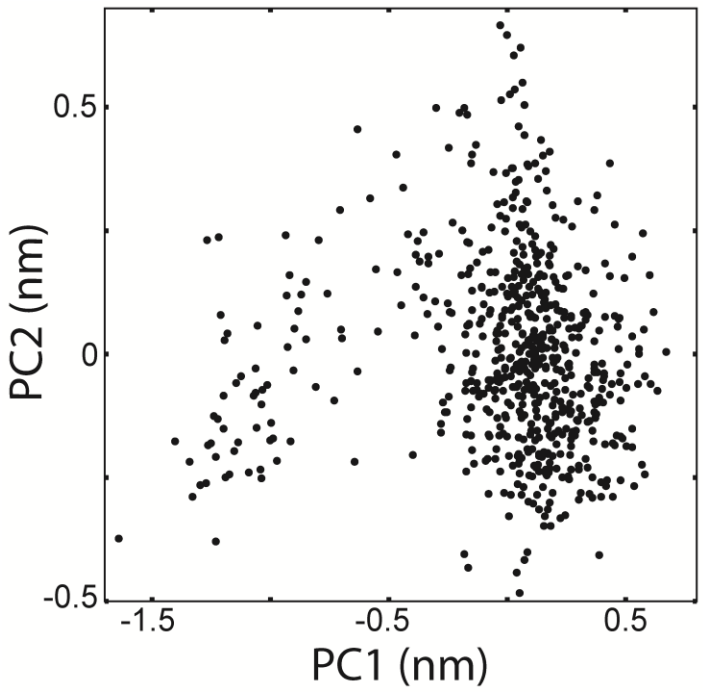

Figure S4. **Principal Component Analysis (PCA) on the RDC derived ERMD ensemble of GB3 reveals higher displacement in the binding site that undergoes conformational exchange.** Projection of 640 different structures of the RDC derived ERMD ensemble of GB3 onto the subspace spanned by first two principle components, PC1 and PC2. The square fluctuations (SF) along PC1 are shown in main text figure 2C.

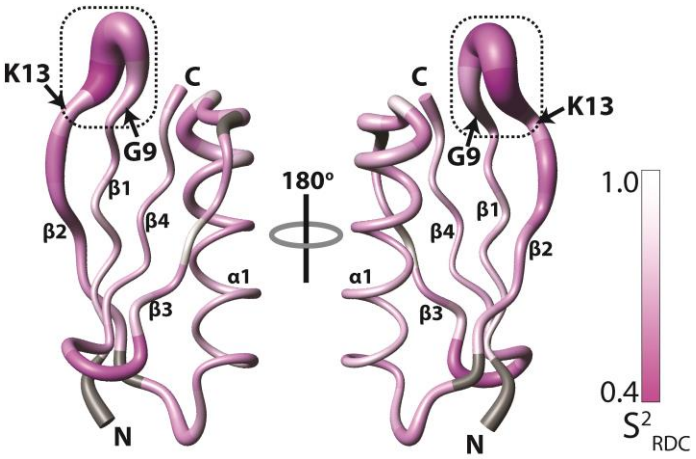

Figure S5. **GB3 ensemble generated from RDC measurements manifests elevated RMSD in the first β-turn region which undergoes conformational exchange.** The mean position of all the backbone Cα atoms from 640 members of the ERMD ensemble is displayed here in tube diagram where the average deviation of all the conformers with respect to the mean position is indicated by the radius of the tube. The tube is colored in magenta according to the RDC derived order parameter(S^2_{RDC}) (Figure 2B in main text). This indicates that the part of the protein having maximum supra-τ_c mobility shows highest RMSD in the ensemble and interestingly this is the region shows RD.

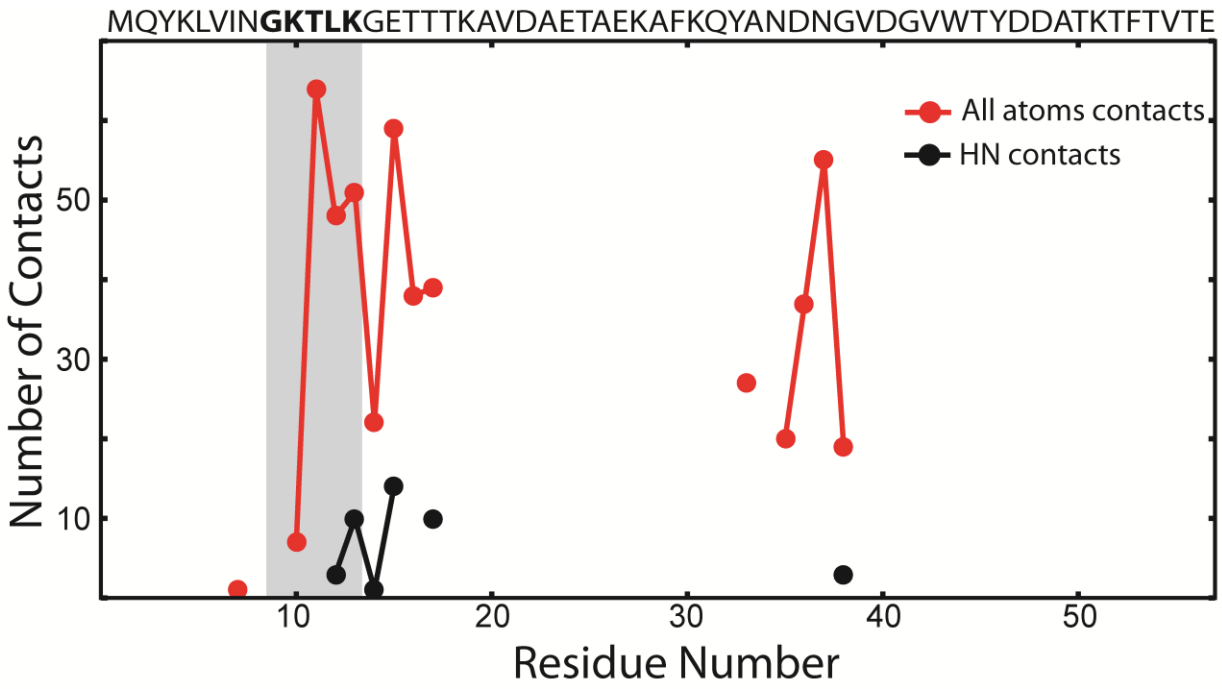

Figure S6. **GB3 interacts with the Fab fragment (MOPC21) predominantly through the first β-turn region which undergoes conformational exchange within the supra-τ_c window.** Number of contacts per residue (within 5 Å) of GB3 with the binding partner (Fab fragment) is calculated for all atoms (red) and backbone amide protons (black). Shaded region indicates the stretch of residues that display RD and it overlaps mostly with the binding site.

Supplementary References

[1] A. M. Gronenborn, D. R. Filpula, N. Z. Essig, A. Achari, *Science* **1991**, *253*, 657–661.
[2] C. Eichmüller, N. R. Skrynnikov, *J. Biomol. NMR* **2005**, *32*, 281–293.
[3] F. A. A. Mulder, R. A. de Graaf, R. Kaptein, R. Boelens, *J. Magn. Reson.* **1998**, *131*, 351–357.
[4] F. Delaglio, S. Grzesiek, G. W. Vuister, G. Zhu, J. Pfeifer, A. Bax, *J. Biomol. NMR* **1995**, *6*, 277–293.
[5] R. Keller, *Optimizing the Process of Nuclear Magnetic Resonance Analysis and Computer Aided Resonance Assignment*, **2004**.
[6] L. Yao, B. Voegeli, D. A. Torchia, A. Bax, *J. Phys. Chem. B* **2008**, *112*, 6045–6056.
[7] R. B. Fenwick, S. Esteban-Martín, B. Richter, D. Lee, K. F. A. Walter, D. Milovanovic, S. Becker, N. A. Lakomek, C. Griesinger, X. Salvatella, *J. Am. Chem. Soc.* **2011**, *133*, 10336–10339.
[8] F. Cordier, L. Nisius, A. J. Dingley, S. Grzesiek, *Nat. Protoc.* **2008**, *3*, 235–241.
[9] G. Cornilescu, J. L. Marquardt, M. Ottiger, *J. Am. Chem. Soc.* **1998**, *120*, 6836–6837.
[10] M. Karplus, *J. Chem. Phys.* **1959**, *30*, 11–15.
[11] B. Vögeli, J. Ying, A. Grishaev, A. Bax, *J. Am. Chem. Soc.* **2007**, *129*, 9377–9385.
[12] J. H. Lee, F. Li, A. Grishaev, A. Bax, *J. Am. Chem. Soc.* **2015**, *137*, 1432–1435.
[13] S. Grzesiek, F. Cordier, V. Jaravine, M. Barfield, *Prog. Nucl. Magn. Reson. Spectrosc.* **2004**, *45*, 275–300.
[14] J. P. Derrick, D. B. Wigley, *J. Mol. Biol.* **1994**, *243*, 906–918.
[15] T. S. Ulmer, B. E. Ramirez, F. Delaglio, A. Bax, *J. Am. Chem. Soc.* **2003**, *125*, 9179–9191.
[16] F. Li, J. H. Lee, A. Grishaev, J. Ying, A. Bax, *Chemphyschem* **2015**, *16*, 572–578.
[17] B. Vögeli, S. Kazemi, P. Güntert, R. Riek, *Nat. Struct. Mol. Biol.* **2012**, *19*, 1053–1057.
[18] G. M. Clore, C. D. Schwieters, *J. Mol. Biol.* **2006**, *355*, 879–886.
[19] S. Olsson, B. R. Voegeli, A. Cavalli, W. Boomsma, J. Ferkinghoff-Borg, K. Lindorff-Larsen, T. Hamelryck, *J. Chem. Theory Comput.* **2014**, *10*, 3484–3491.
[20] T. M. Sabo, C. A. Smith, D. Ban, A. Mazur, D. Lee, C. Griesinger, *J. Biomol. NMR* **2014**, *58*, 287–301.
[21] P. Pelupessy, E. Chiarparin, R. Ghose, G. Bodenhausen, *J. Biomol. NMR* **1999**, *14*, 277–280.
[22] B. Reif, M. Hennig, C. Griesinger, *Science* **1997**, *276*, 1230–1233.
[23] R. B. Fenwick, S. Esteban-Martín, X. Salvatella, *J. Phys. Chem. Lett.* **2010**, *1*, 3438–3441.
[24] L. Yao, B. Voegeli, J. Ying, A. Bax, *J. Am. Chem. Soc.* **2008**, *130*, 16518–16520.
[25] D. Lee, C. Hilty, G. Wider, K. Wüthrich, *J. Magn. Reson.* **2006**, *178*, 72–76.
[26] S. Neal, A. M. Nip, H. Zhang, D. S. Wishart, *J. Biomol. NMR* **2003**, *26*, 215–240.
[27] Y. Shen, A. Bax, *J. Biomol. NMR* **2007**, *38*, 289–302.
[28] D. Ban, M. Funk, R. Gulich, D. Egger, T. M. Sabo, K. F. A. Walter, R. B. Fenwick, K. Giller, F. Pichierri, B. L. de Groot, et al., *Angew. Chem. Int. Ed. Engl.* **2011**, *50*, 11437–11440.